

# ORCA: A Global Ocean Emulator for Multi-year to Decadal Predictions

Zijie Guo<sup>1</sup>, Pumeng Lyu<sup>1</sup>, Fenghua Ling<sup>2,1</sup>, Jing-Jia Luo<sup>2</sup>,  
Niklas Boers<sup>3</sup>, Wanli Ouyang<sup>1</sup>, Lei Bai<sup>1\*</sup>

<sup>1</sup>Shanghai Artificial Intelligence Laboratory.

<sup>2</sup>Nanjing University of Information Science and Technology.

<sup>3</sup>Technical University of Munich, Potsdam Institute for Climate Impact Research.

\*Corresponding author(s). E-mail(s): [baisanshi@gmail.com](mailto:baisanshi@gmail.com);

## Abstract

Ocean dynamics plays a crucial role in driving global weather and climate patterns. Accurate and efficient modeling of ocean dynamics is essential for improved understanding of complex ocean circulation and processes, for predicting climate variations and their associated teleconnections, and for addressing the challenges of climate change. While great efforts have been made to improve numerical Ocean General Circulation Models (OGCMs), accurate forecasting of global oceanic variations for multi-year remains to be a long-standing challenge. Here, we introduce ORCA (Oceanic Reliable foreCAst), the first data-driven model predicting global ocean circulation from multi-year to decadal time scales. ORCA accurately simulates the three-dimensional circulations and dynamics of the global ocean with high physical consistency. Hindcasts of key oceanic variables demonstrate ORCA's remarkable prediction skills in predicting ocean variations compared with state-of-the-art numerical OGCMs and abilities in capturing occurrences of extreme events at the subsurface ocean and ENSO vertical patterns. These results demonstrate the potential of data-driven ocean models for providing cheap, efficient, and accurate global ocean modeling and prediction. Moreover, ORCA stably and faithfully emulates ocean dynamics at decadal timescales, demonstrating its potential even for climate projections. The model will be available at <https://github.com/OpenEarthLab/ORCA>.

**Keywords:** Ocean Modeling, Multi-year Prediction, Deep Learning

# 1 Introduction

The global oceans encompass over 70% of the Earth’s surface and stand as the main component of Earth’s hydrosphere. A significant portion of incoming solar radiation is absorbed by the oceans, constituting considerable energy storage. Ocean currents act as global-scale conveyor belt to distribute this energy from the tropics to the polar regions, driving weather patterns and teleconnections around the globe. Moreover, the oceans contribute substantially to the global water cycle. The oceans hence play a crucial role in the Earth’s energy and water balance, as well as multi-year to decadal climate variations and associated teleconnections, making them an indispensable part of the climate system.

Over the past decades, complicated ocean general circulation models (OGCMs) have been developed to simulate ocean currents, temperature, salinity distributions, and other physical processes by numerically integrating the governing partial differential equations on discretized spatial grid [1]. However, due to the computational costs of solving these equations numerically, the spatial resolution remains coarse and many small-scale yet highly relevant processes cannot be explicitly resolved. Consequently, predictions made by OGCMs remain subject to substantial uncertainties [2, 3].

Recently, deep learning (DL) [4] methods have shown remarkable advances in simulating complex atmospheric circulation systems in weather forecasting up to about two weeks in advance [5–9]. Notably, these DL-based models exhibit improved forecasting skills compared to state-of-the-art atmospheric GCMs [10, 11] while being computationally orders of magnitude more efficient. These advancements have also opened new avenues for ocean modeling. Although there have been some previous attempts at ocean modeling, such as the utilization of a Fourier Neural Operator (FNO) [12] based model to simulate the baroclinic double gyre for multi-decadal timescales [13], the existing works primarily concentrate on either the regional ocean [14], specific variables [15, 16], relatively short timescales [17, 18], or some combination thereof [19]. Long-term modeling of the global oceans has yet to be extensively explored.

Here, we present ORCA (Oceanic Reliable foreCAst), the first data-driven model for multi-year to decadal predictions of the global ocean circulation and states. Built on an encoder-fusion-decoder scheme and leveraging a time-based Mixture-of-Experts (MoE) [20] attention block and a novel atmosphere condition fusion module, ORCA stably and accurately simulates the global oceans dynamics for three dimensions and multiple key variables (e.g., salinity, potential temperature, and velocity) from multi-year to decadal timescales. Using reanalysis data for the past four decades, we compare ORCA’s predictions of key oceanic variables with other available dynamical global forecast systems. ORCA produces physically consistent results, exhibits exceptional prediction skills, and strongly outperforms other numerical OGCMs. In particular, ORCA shows excellent modeling capabilities at multi-year timescales, as evidenced by the skillful forecast of key oceanic variables. The remarkable prediction of subsurface heatwaves and highly consistent vertical patterns further prove its proficiency in three-dimensional ocean modeling. Additionally, a decadal prediction experiment demonstrates the stability of ORCA in long-term emulation. These results underscore the potential of data-driven and artificial intelligence methods to

revolutionize ocean modeling for improved predictions of ocean dynamics and associated teleconnection patterns up to decadal time scales, and promise substantial improvements in the computational efficiency of climate models.

## 2 Results

ORCA can realistically simulate multi-level global ocean dynamics, with monthly forecasting horizons ranging from one month to years. It can skilfully predict global ocean fields with one-degree spatial resolution and up to 1000 meters below sea level. The simulated oceanic fields include two surface variables, i.e., sea surface temperature (tos) and sea surface height above the geoid (zos), and four multi-level oceanic variables, i.e., salinity (so), potential temperature (thetao), zonal velocity (uo), and meridional velocity (vo). In addition to these six oceanic variables, the zonal and meridional surface wind stress (tauu and tauv) are also incorporated as the atmospheric forcing variables for air-sea coupling processes. To examine our model’s performances, data from the NCEP Global Ocean Data Assimilation System (GODAS) [21] is used as observational ground truth in order to evaluate the skills.

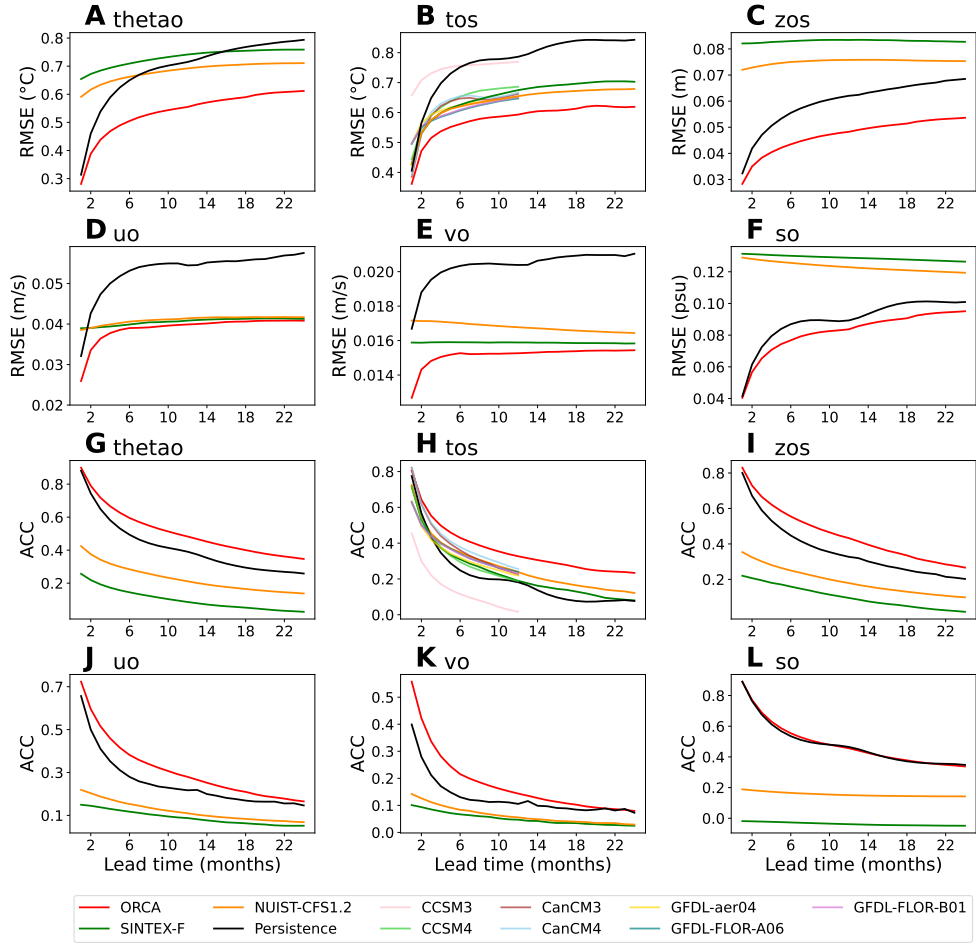
### 2.1 Multi-year Forecast Skills

Fig. 1 presents the global forecasts skills of our ORCA model in comparison with several state-of-the-art ocean-atmosphere coupled general circulation models, including SINTEX-F [22], NUIST-CFS1.2 [23], and seven models of the North American Multi-Model Ensemble (NMME) [24]. Root Mean Square Error (RMSE) (Fig. 1 A-F) and Anomaly Correlation Coefficient (ACC) (Fig. 1 G-L) are assessed here with assessment period spanning from 1985 to 2018 (skills for multi-level variables are averaged over depth, see Supplementary Fig. S1 and Fig. S2 for skills at each depth). As can be observed, ORCA demonstrates superior forecasting skills compared to the dynamical coupled models, maintaining better overall performance throughout the 24-month forecast period. ORCA’s forecasting skill at the 24-month lead is even better than most dynamical models at the 12-month lead, thus effectively doubling the forecast horizon.

### 2.2 Oceanic Variation Emulation

As the first data-driven AI model for multi-year to decadal ocean forecasts, ORCA displays the advantage of capturing evolved oceanic signals compared with state-of-the-art dynamical models. Here, we show that ORCA not only accurately captures occurrences of extreme events at subsurface oceans, but also ensures exact ocean behaviors in mesopelagic zone at 200-1000m depth in Niño3.4 region. These results further demonstrate the ability of ORCA to detect irregular climate oscillations.

**Subsurface Marine Heatwaves Forecast.** Marine heatwaves (MHWs) are often tracked and forecasted at the surface due to the widespread availability of surface temperature fields [25, 26]. However, considering the significant impacts of MHW below the ocean surface [27, 28], there is a growing recognition of the need to improve subsurface MHW forecasts. Here, monthly-scale subsurface MHWs are defined based



**Fig. 1 The comparison of the forecasting skill for six oceanic variables.** The testing period spans from 1985 to 2018. The x-axis represents the forecast lead time with an interval of one month. (A-F) The global average of the Root Mean Square Error (RMSE) between predictions and observations for the anomalies of six variables on each grid (the lower the better). (G-L) As in (A-F), but for the Anomaly Correlation Coefficient (ACC) skill (the higher the better).

on ocean heat content following previous works [29] (please refer to Section 4.4 for the detailed definition and see Supplementary Fig. S3 for the results of surface MHWs). We use the Symmetric Extremal Dependence Index (SEDI) [30] as the metric, which is commonly used for extreme events forecast evaluation and higher SEDI means better performance.

Fig. 2 E shows the frequency distribution of MHWs calculated using the GODAS data. While a few regions have a high frequency of MHWs occurrence, the majority of regions have a frequency around ten percent, which corresponds to the 90 percent threshold (cf. Section 4.4). Fig. 2 B-D and F-I illustrate the subsurface MHWs forecast performance for seven regions with a relatively high frequency of occurrence,

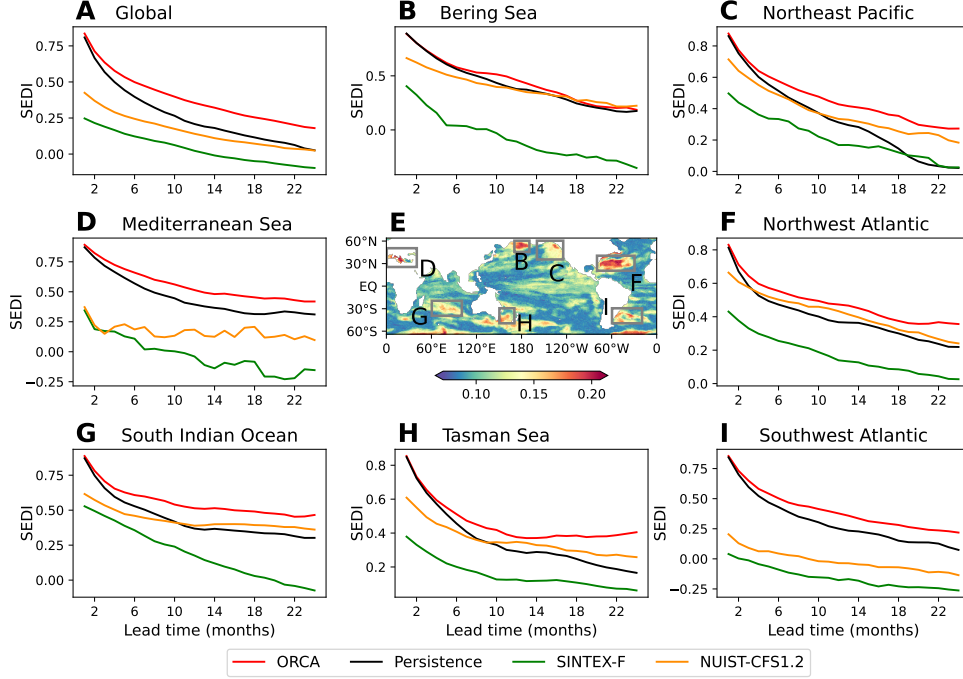


**Fig. 2 Forecast skills of subsurface marine heatwaves.** (A-D, F-I) The average SEDI for global and seven regions with a relatively high frequency of heatwave occurrences, the higher the better. The x-axis represents the forecast lead time. (E) Global distribution of the frequency of heat wave events based on GODAS. The area in the gray box corresponds to the surrounding subgraph identified by the black letter.

including the Berling Sea, Northeast Pacific, Mediterranean Sea, NorthWest Atlantic, South Indian Ocean, Tasman Sea, and Southwest Atlantic. ORCA exhibits the highest performance up to 24 months for all the regions considered, surpassing SINTEX-F, NUIST-CFS1.2, and the persistence forecast. This result further reinforces ORCA’s strong modeling capabilities in the subsurface layer, indicating its effectiveness in forecasting extreme temperature events below the ocean surface.

**ENSO Vertical Pattern.** The ability of the model to predict the structure below the surface serves as an indicator of its accuracy in modeling ocean dynamics. Therefore, we further investigate the vertical potential temperature patterns in the Niño3.4 region (170°-120°W, 5°S-5°N), which is a critical ocean area that has been extensively applied for ENSO studies [31, 32].

Fig. 3 depicts the temporal evolution of the Nino3.4 area-averaged potential temperature anomalies from surface to 1000m depth. The surface anomalies exhibit an alternating pattern of warm and cold phases, which indicate El Niño or La Niña events [31]. It is noteworthy that both ORCA and NUIST-CFS1.2 capture the alternating phases of warm and cold anomalies in the Niño3.4 region at different lead months (see also Supplementary Fig. S4 regarding the results of Niño3.4 Index prediction). However, the depth-average RMSE and ACC skills, as shown in Fig. 3 C-D, indicates that



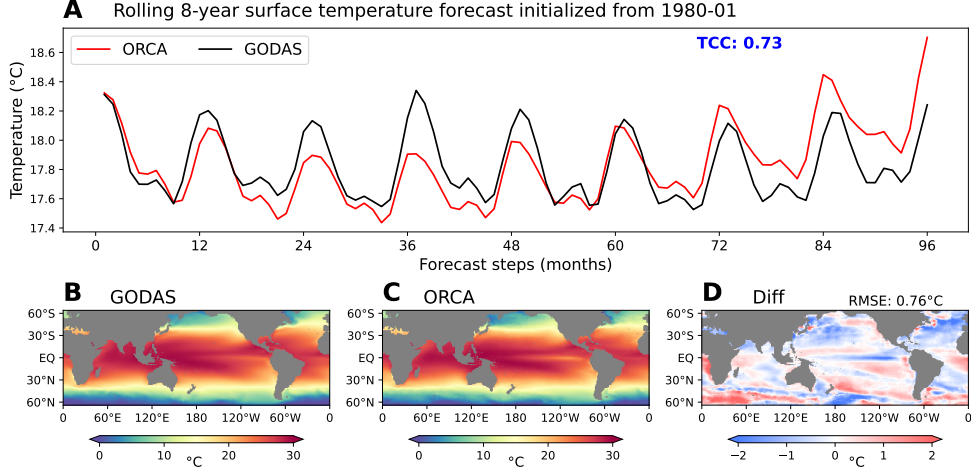


**Fig. 4 Long-term rolling forecast of sea surface temperatures (SST).** (A) The 8-year rolling sea surface temperature forecast of ORCA compared to GODAS observations. The x-axis and y-axis represent the forecast lead months and global averaged SST, respectively. The TCC indicates the Temporal Correlation Coefficient. (B-C) The spatial distribution of 8-year mean SST from GODAS and ORCA forecast, respectively. (D) The difference between ORCA forecast and GODAS (i.e. ORCA forecast minus GODAS).

ORCA exhibits superior forecasting capabilities compared to NUIST-CFS1.2. This suggests that ORCA performs better in representing the temperature patterns below the surface.

It is also evident from Fig. 3 E that NUIST-CFS1.2 encounters a significant forecasting barrier at approximately 300m depth and nearly loses its predictive skill. Additionally, a spurious temporal shift is observed. Prior to the year 2000, predominantly cold anomalies are prevalent, while after the year 2000, predominantly warm anomalies are observed. This bias further confirms the mediocre performance of NUIST-CFS1.2 as shown in Fig. 1 G. In contrast, ORCA still demonstrates good performance at both surface and deep layers, revealing that OCRA learns physically meaningful ocean dynamics.

### 2.3 Towards Decadal Prediction

To investigate the possibility of conducting long lead forecast by ORCA, we conduct long-range rolling predictions spanning 8 years and starting from the initial field of January 1980 (the first available time for GODAS). This experiment allows us to assess the model’s performance over an extended period and evaluate its consistency and accuracy in capturing long-term trends and variations.

While many dynamical models often suffer from instability [33, 34], our results show that ORCA runs stably over this decadal time scale. Fig. 4 A depicts the variation of global average surface temperature with forecast lead months. It can be observed that the ORCA forecast exhibits a slight cold bias during approximately the first 5 years and then gradually shifts towards warmer temperatures. Nevertheless, there is a

remarkable consistency between the forecast of ORCA and GODAS observations, as evidenced by a Temporal Correlation Coefficient (TCC) of 0.73.

The 8-year average sea surface temperature on each grid cell is illustrated in Fig. 4 B-C. Despite the cold or warm biases in different regions, as shown in Fig. 4 D, it is noteworthy that there remains a high spatial consistency, as indicated by a small global mean RMSE of 0.76°C. The biases in the forecasted sea surface temperature are generally smaller compared to many of current dynamical models [35, 36].

### 3 Discussion

In this paper, we present the first data-driven global ocean circulation forecasting model ORCA for multi-year to decadal predictions. By training with historical simulations from 20 models in the CMIP6, ORCA exhibits an extraordinary forecast skill almost for all considered variables, except for slightly inferior ACC skills for the salinity when the lead time exceeds eleven months. One possible reason is that salinity exhibits relatively small variations compared to other variables, making the persistence model a strong baseline. The performance of ORCA in capturing subsurface dynamics underscores its potential for accurately predicting and monitoring subsurface variations. Furthermore, a decadal forecast of global surface temperature with high spatial-temporal consistency demonstrates the ORCA’s ability to emulate ocean variations. In particular, this result shows that ORCA can run stably over a decade, making it a promising candidate also for climate projections.

Due to the insufficient observed monthly data, we had to train ORCA on simulated data from a large ensemble of state-of-art climate models, which exhibit biases. Therefore, there is still room for further development of more effective transfer learning approaches, tailored to the specific requirements of such a large model. In addition, we are particularly interested in incorporating external constraints such as carbon dioxide concentrations and physical laws into deep learning models in our future studies.

## 4 Methods

### 4.1 Datasets

Historical simulations from 20 models that participated in the Coupled Model Inter-comparison Project phase 6 (CMIP6) [37] are adopted for training (see Supplementary Table S1). And the data before 1980 from reanalysis datasets Simple Ocean Data Assimilation (SODA) [38] and Ocean Reanalysis System 5 (ORAS5) [39] are used for model evaluation and parameters tuning. After training, we conduct independent testing of ORCA with reanalysis data produced by NCEP Global Ocean Data Assimilation System (GODAS) [21] from 1980 to 2023. Hindcast results from SINTEX-F [22], NUIST-CFS1.2 [23] and seven models of the North American Multi-Model Ensemble (NMME) [24] are used for performances comparison.

For easier modeling, all data mentioned above are interpolated into the regular grid (63.5°S - 63.5°N, 0.5° - 359.5°E) with the resolution of 1° (128 × 360 grid points). Also, the multi-level variables are interpolated into pre-defined depths, including 16 layers in depth (see Table 1).



Vertical Level	Variables
Surface	tos, zos, tauu, tauv
16 layers in depth	thetao, uo, vo, so

**Table 1** Variables modeled by ORCA. Abbreviations are given as follows. tos: surface temperature, zos: surface height above the geoid, tauu (tauv) zonal (meridional) wind stress, thetao: potential temperature, uo and vo: zonal and meridional velocity, so: salinity. Sixteen layers in depth include 10m, 15m, 30m, 50m, 75m, 100m, 125m, 150m, 200m, 250m, 300m, 400m, 500m, 600m, 800m, and 1000m.

## 4.2 Problem Formulation

ORCA is a skillful data-driven climate model that aims to predict the future ocean states based on the current ocean and atmosphere states. Formally, given the input ocean variables  $O^t \in \mathbb{R}^{N_o \times N_{\text{lat}} \times N_{\text{lon}}}$ , atmosphere variables (e.g, wind stress)  $A^t \in \mathbb{R}^{N_a \times N_{\text{lat}} \times N_{\text{lon}}}$ , lead time  $\Delta t$ , and ocean-land mask  $M$ , ORCA is trained to produce the future ocean states  $\hat{O}^{t+\Delta t}$ , as shown in the Eq. 1,

$$\hat{O}^{t+\Delta t} = \text{ORCA}(O^t, A^t, \Delta t, M), \quad (1)$$

where  $N_o$  denotes the number of ocean predictands,  $N_a$  denotes the number of atmosphere variables,  $N_{\text{lat}}$  and  $N_{\text{lon}}$  denote the number of grids in latitude and longitude directions. In this study, we set  $N_o = 66$ ,  $N_a = 2$ ,  $N_{\text{lat}} = 128$ ,  $N_{\text{lon}} = 360$ ,  $\Delta t \in \{1, 2, \dots, K\}$ , where  $K$  is the maximum number of step during the model training and the time interval is one month. Since the model becomes more difficult to converge when  $K$  gets larger, we set  $K = 6$  during the model training phase. To generate forecasts with a lead time larger than  $K$  steps, we feed the model with the latest outputs  $\hat{O}^{t+K}$  to get  $\hat{O}^{t+K+\Delta t}$  during inference, as shown in Eq. 2. In this way, we can autoregressively predict oceanic states at any number of steps.

$$\hat{O}^{t+K+\Delta t} = \text{ORCA}(\hat{O}^{t+K}, A^t, \Delta t, M). \quad (2)$$

## 4.3 Metrics

**RMSE** (Root Mean Square Error) is a commonly used metric for evaluating how close a prediction is to the observation. Given the predicted values  $\hat{O}^{t+\Delta t}$  and the observed values  $O^{t+\Delta t}$ , the RMSE can be calculated as follows:

$$\text{RMSE}(v, \Delta t) = \sqrt{\frac{1}{N_{\text{lat}} \times N_{\text{lon}}} \sum_{i,j} (\hat{O}_{v,i,j}^{t+\Delta t} - O_{v,i,j}^{t+\Delta t})^2}, \quad (3)$$

where  $v$  denotes the specific variable or layer of multi-level variables.

**ACC** (Anomaly Correlation Coefficient) is a statistical measure used to evaluate how well a model is able to capture and reproduce the patterns and phases of observed

anomalies. The ACC of the prediction on a specific grid can be computed as follows:

$$\text{ACC}(v, i, j, \Delta t) = \frac{\sum_t (\hat{O}_{v,i,j}^{t+\Delta t} - \hat{C}_{v,i,j}^{m_{t+\Delta t}})(O_{v,i,j}^{t+\Delta t} - C_{v,i,j}^{m_{t+\Delta t}})}{\sqrt{\sum_t (\hat{O}_{v,i,j}^{t+\Delta t} - \hat{C}_{v,i,j}^{m_{t+\Delta t}})^2 \sum_t (O_{v,i,j}^{t+\Delta t} - C_{v,i,j}^{m_{t+\Delta t}})^2}}, \quad (4)$$

where  $\hat{C}$  and  $C$  denote the forecast and observed climatology,  $m_{t+\Delta t}$  denotes the month corresponding to the time  $t + \Delta t$ . To obtain the ACC value for a region, we simply average the ACC of each grid within the region.

**SEDI** (Symmetric Extremal Dependence Index) [30] is a measure for rare binary event forecast with several advantages, including non-degenerate, base-rate independent, asymptotically equitable, and so on. In this study, we use SEDI to assess the forecast performance of subsurface marine heatwaves. It is defined as follows:

$$\text{SEDI} = \frac{\log F - \log H - \log(1 - F) + \log(1 - H)}{\log F + \log H + \log(1 - F) + \log(1 - H)}, \quad (5)$$

where  $H$  is the hit rate (true positive rate) and  $F$  is the false alarm rate (false positive rate). SEDI has a range from  $-1$  to  $1$ , and a higher value indicates better performance.

#### 4.4 Subsurface MHWs Definition

In this study, subsurface MHWs are defined with ocean heat content (OHC) following that of [29]. The OHC can be calculated as follows:

$$\text{OHC} = c_p \rho \int_{z_1=0\text{m}}^{z_2=300\text{m}} T(z) dz, \quad (6)$$

where  $c_p$  is the specific heat capacity of seawater ( $3996 \text{ J}/(\text{kg}\cdot\text{C})$ ),  $\rho$  is the density ( $1026 \text{ kg}/\text{m}^3$ ), and  $T(z)$  is the potential temperature at the depth  $z$ . We first calculate the OHC anomalies from 1985 to 2018 and the seasonal 90th percentile during the first 30 years. Then, an MHW event is identified when the anomalies are greater than the 90th percentile [26, 40, 41].

#### 4.5 Model

Inspired by FengWu [9], ORCA is established on an encoder-fusion-decoder scheme as illustrated in Fig. 5. The input ocean variables  $O^t$  and atmosphere variables  $A^t$  are respectively encoded by Ocean Encoders and an Atmosphere Encoder. Then, the encoded hidden states are fused by a Fusion Module. Finally, Ocean Decoders decode the fused hidden states into the predicted ocean states.

**Ocean Encoders and Decoders** consist of several ocean variable specific encoders and decoders. As ORCA treats each ocean variable as a modality, each variable corresponds to an encoder and decoder module similar to FengWu. For each variable, the encoder module first patchifies it with a patch embedding module, which is a common operation in computer vision [42]. Several consecutive local attention blocks then

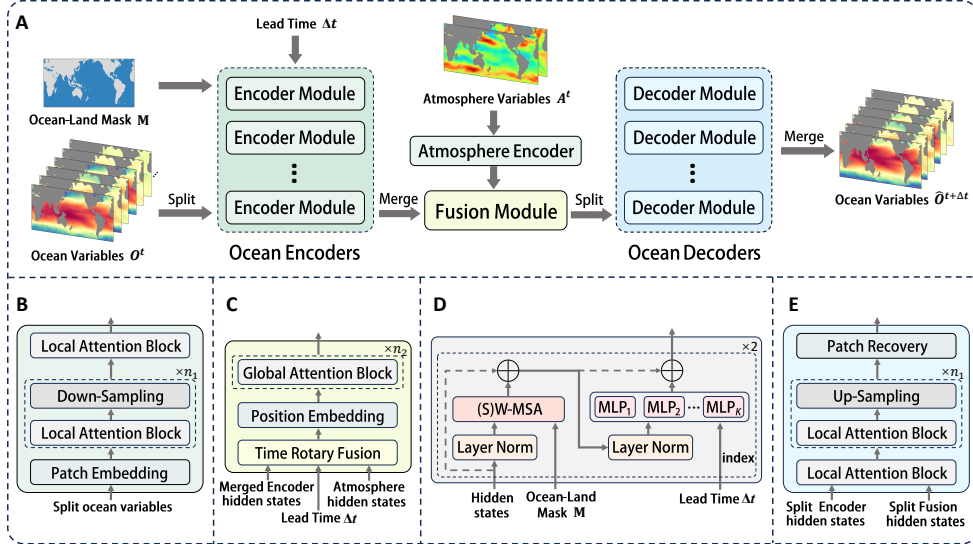


**Fig. 5 Architecture of the ORCA model.** (A) ORCA consists of several ocean encoders, an atmosphere encoder, a fusion module, and several ocean decoders (skipping connections between each encoder module and decoder module are not shown for brevity). The inputs include current ocean and atmosphere variables  $O^t$  and  $A^t$ , ocean-land mask  $M$ , and lead time  $\Delta t$ . The outputs are future ocean states specified by  $\Delta t$ . (B) Structure of the encoder module. (C) Structure of the fusion module. (D) Structure of the attention block. Local and global attention blocks share the same structure, but only with the difference in window size. (E) Structure of the decoder module.

extract the high-level information. To capture features at different spatial scales while saving memory, down-sampling is conducted after every attention block except the last one following the implementation in Swin Transformer [43]. The decoder module has an inverse process like the encoder.

**Fusion Module** takes the merged ocean hidden states encoded by all encoder modules, atmosphere hidden states encoded by the atmosphere encoder, and the lead time  $\Delta t$  as inputs. Inspired by the commonly used Rotary Position Embedding (RoPE) [44] in natural language processing, we transfer the position encoding to time encoding and propose the Time Rotary Fusion Module.

Let  $\mathbf{x}_o, \mathbf{x}_a \in \mathbb{R}^d$  denotes the hidden states vector of a single grid in ocean and atmosphere hidden states respectively, where  $d$  is hidden dims. We can get the rotated atmosphere vector  $\mathbf{x}'_a = \mathbf{R}_{\Theta, \Delta t}^d \mathbf{x}_a$ , where  $\mathbf{R}_{\Theta, \Delta t}^d$  is the rotary matrix with pre-defined

parameters  $\Theta = \{\theta_i = 10000^{-2(i-1)/d}, i \in [1, 2, \dots, d/2]\}$  defined as follows:

$$\mathbf{R}_{\Theta, \Delta t}^d = \begin{pmatrix} \cos \theta_1 \Delta t & -\sin \theta_1 \Delta t & 0 & 0 & \cdots & 0 & 0 \\ \sin \theta_1 \Delta t & \cos \theta_1 \Delta t & 0 & 0 & \cdots & 0 & 0 \\ 0 & 0 & \cos \theta_2 \Delta t & -\sin \theta_2 \Delta t & \cdots & 0 & 0 \\ 0 & 0 & \sin \theta_2 \Delta t & \cos \theta_2 \Delta t & \cdots & 0 & 0 \\ \vdots & \vdots & \vdots & \vdots & \ddots & \vdots & \vdots \\ 0 & 0 & 0 & 0 & \cdots & \cos \theta_{d/2} \Delta t & -\sin \theta_{d/2} \Delta t \\ 0 & 0 & 0 & 0 & \cdots & \sin \theta_{d/2} \Delta t & \cos \theta_{d/2} \Delta t \end{pmatrix} \quad (7)$$

Then, the fused hidden vector  $\mathbf{x}_f$  can be calculated as follows:

$$\mathbf{x}_f = \mathbf{x}_o + \langle \mathbf{x}_o, \mathbf{x}'_a \rangle \cdot \mathbf{x}_a, \quad (8)$$

where  $\langle \cdot \rangle$  denotes the inner product. When  $\Delta t$  gets larger, the relation between  $\mathbf{x}_o$  and  $\mathbf{x}_a$  gets weaker, quantified by  $\langle \mathbf{x}_o, \mathbf{x}'_a \rangle$  in Eq. 8 (see also the original paper [44] for a detailed theoretical demonstration). With the Time Rotary Fusion Module, we can fuse the current input ocean hidden states and the initial atmosphere hidden states (current and initial conditions can be at a different time when doing autoregressive forecast), which avoids the challenging forecast of the wind stress [45].

In order to further facilitate the model in extracting global information, position embedding [42] and several consecutive global attention blocks are added after fusion. **Attention Block** is mainly based on Swin Transformer [43]. It contains two successive sub-blocks. The first sub-block employs window-based multi-head self-attention (W-MSA) to capture the local information, while the subsequent sub-block uses shifted W-MSA (SW-MSA) for interactions across the windows. We introduce the ocean-land mask  $M$  to force the model to focus only on the ocean realm, similar to XiHe [17]. To reduce the forecast steps, we replace the single MultiLayer Perceptron (MLP) module with a group of MLPs like the prevailing module Mixture-of-Experts (MoE) [20] used in natural language processing and use the lead time  $\Delta t$  to index which MLP to use, which alleviates the accumulation of errors and saves the memory cost. The overall attention block is computed as follows:

$$\begin{aligned} \hat{Z}^l &= \text{W-MSA}(\text{LN}(Z^{l-1}), M) + Z^{l-1}, \\ Z^l &= \text{MLP}_{\Delta t}(\text{LN}(\hat{Z}^l)) + \hat{Z}^l, \\ \hat{Z}^{l+1} &= \text{SW-MSA}(\text{LN}(Z^l), M) + Z^l, \\ Z^{l+1} &= \text{MLP}_{\Delta t}(\text{LN}(\hat{Z}^{l+1})) + \hat{Z}^{l+1}, \end{aligned} \quad (9)$$

where LN denotes the Layer Normalization [46],  $M$  is the ocean-land mask,  $\hat{Z}^l$  and  $Z^l$  represent the output features of the (S)W-MSA and MLP for block  $l$ , respectively.

The attention used inside the (S)W-MSA is defined as follows:

$$\text{Attention}(Q, K, V) = \text{SoftMax}(QK^T/\sqrt{d} + M)V, \quad (10)$$

where  $Q$ ,  $K$ , and  $V$  represent the query, key, and values vectors, and  $d$  is the hidden dims. Instead of using the relative position bias [43], we employ the RoPE [44] to implicitly learn the relative position information. Moreover, the ocean-land mask  $M$  is added to the attention matrix to mask the land realm.

**Atmosphere Encoder** shares the same structure with the ocean encoder module but only uses one MLP in the attention sub-block as we do not forecast the atmosphere variables but employ the Time Rotary Fusion Module as mentioned above.

## 4.6 Training Details

ORCA is implemented with the Pytorch framework and trained with 4 Nvidia A100 GPUs within 12 hours using a total batch size of 32. The RMSE loss is used as the optimization target, which is defined as follows:

$$\mathcal{L}_{\text{RMSE}} = \sqrt{\frac{1}{N_o \times N_{\text{lat}} \times N_{\text{lon}}} \sum_{v,i,j} (\hat{O}_{v,i,j}^{t+\Delta t} - O_{v,i,j}^{t+\Delta t})^2}. \quad (11)$$

We adopt the Adam [47] as the optimizer using the following parameters:  $\beta_1 = 0.9$ ,  $\beta_2 = 0.95$ ,  $\epsilon = 1e^{-6}$  and  $L_2$  weight decay of 0.1. The learning rate is warmed up with a ratio of 0.1 to a maximum value of  $2e^{-4}$ , after which the cosine annealing is applied. Moreover, in order to realize the ensemble forecast, ten identical models are trained only with the difference of initial random seeds.

## Acknowledgements

We would like to express our gratitude to the World Climate Research Programme for coordinating and promoting CMIP6 and Earth System Grid Federation (ESGF) for archiving the data and providing access. We acknowledge NOAA MAPP, NSF, NASA, and the DOE for supporting the phase-2 NMME project. We acknowledge the Nanjing University of Information Science and Technology for providing NUIST-CFS1.2 and SINTEX-F data. We acknowledge the NOAA Physical Sciences Laboratory for their GODAS data, the University of Maryland and Texas A&M University for their SODA2 data, and the European Centre for Medium-Range Weather Forecasts for their ORAS5 data.

We acknowledge the Research Support, IT, and Infrastructure team at the Shanghai AI Laboratory for their valuable assistance in providing computation resources and network support throughout this research project. We also acknowledge the support of F Ling and J-J Luo, who are funded by the National Key Research and Development Program of China (No. 2020YFA0608000).

## References

- [1] Griffies, S.M., Böning, C., Bryan, F.O., Chassignet, E.P., Gerdes, R., Hasumi, H., Hirst, A., Treguier, A.-M., Webb, D.: Developments in ocean climate modelling. *Ocean Modelling* **2**(3-4), 123–192 (2000)
- [2] Bauer, P., Thorpe, A., Brunet, G.: The quiet revolution of numerical weather prediction. *Nature* **525**(7567), 47–55 (2015)
- [3] Palmer, T., Shutts, G., Hagedorn, R., Doblas-Reyes, F., Jung, T., Leutbecher, M.: Representing model uncertainty in weather and climate prediction. *Annu. Rev. Earth Planet. Sci.* **33**, 163–193 (2005)
- [4] LeCun, Y., Bengio, Y., Hinton, G.: Deep learning. *nature* **521**(7553), 436–444 (2015)
- [5] Bi, K., Xie, L., Zhang, H., Chen, X., Gu, X., Tian, Q.: Pangu-weather: A 3d high-resolution model for fast and accurate global weather forecast. *arXiv preprint arXiv:2211.02556* (2022)
- [6] Beucler, T., Ebert-Uphoff, I., Rasp, S., Pritchard, M., Gentine, P.: Machine learning for clouds and climate. *Clouds and their climatic impacts: Radiation, circulation, and precipitation*, 325–345 (2023)
- [7] Ling, F., Ouyang, L., Larbi, B.R., Luo, J.-J., Han, T., Zhong, X., Bai, L.: Is artificial intelligence providing the second revolution for weather forecasting? *arXiv preprint arXiv:2401.16669* (2024)
- [8] Lam, R., Sanchez-Gonzalez, A., Willson, M., Wirnsberger, P., Fortunato, M., Alet, F., Ravuri, S., Ewalds, T., Eaton-Rosen, Z., Hu, W., et al.: Graphcast: Learning skillful medium-range global weather forecasting. *arXiv preprint arXiv:2212.12794* (2022)
- [9] Chen, K., Han, T., Gong, J., Bai, L., Ling, F., Luo, J.-J., Chen, X., Ma, L., Zhang, T., Su, R., et al.: Fengwu: Pushing the skillful global medium-range weather forecast beyond 10 days lead. *arXiv preprint arXiv:2304.02948* (2023)
- [10] Charney, J.G., Fjørtoft, R., Neumann, J.v.: Numerical integration of the barotropic vorticity equation. *Tellus* **2**(4), 237–254 (1950)
- [11] Lynch, P.: The origins of computer weather prediction and climate modeling. *Journal of computational physics* **227**(7), 3431–3444 (2008)
- [12] Li, Z., Kovachki, N., Azizzadenesheli, K., Liu, B., Bhattacharya, K., Stuart, A., Anandkumar, A.: Fourier neural operator for parametric partial differential equations. *arXiv preprint arXiv:2010.08895* (2020)
- [13] Bire, S., Lütjens, B., Azizzadenesheli, K., Anandkumar, A., Hill, C.N.: Ocean

- emulation with fourier neural operators: Double gyre. Authorea Preprints (2023)
- [14] Subel, A., Zanna, L.: Building ocean climate emulators. arXiv preprint arXiv:2402.04342 (2024)
- [15] Taylor, J., Feng, M.: A deep learning model for forecasting global monthly mean sea surface temperature anomalies. *Frontiers in Climate* **4**, 932932 (2022)
- [16] Ning, D., Vetrova, V., Bryan, K.R.: Graph-based deep learning for sea surface temperature forecasts. arXiv preprint arXiv:2305.09468 (2023)
- [17] Wang, X., Wang, R., Hu, N., Wang, P., Huo, P., Wang, G., Wang, H., Wang, S., Zhu, J., Xu, J., et al.: Xihe: A data-driven model for global ocean eddy-resolving forecasting. arXiv preprint arXiv:2402.02995 (2024)
- [18] Xiong, W., Xiang, Y., Wu, H., Zhou, S., Sun, Y., Ma, M., Huang, X.: Ai-goms: Large ai-driven global ocean modeling system. arXiv preprint arXiv:2308.03152 (2023)
- [19] Chattopadhyay, A., Gray, M., Wu, T., Lowe, A.B., He, R.: Oceannet: A principled neural operator-based digital twin for regional oceans. arXiv preprint arXiv:2310.00813 (2023)
- [20] Shazeer, N., Mirhoseini, A., Maziarz, K., Davis, A., Le, Q., Hinton, G., Dean, J.: Outrageously large neural networks: The sparsely-gated mixture-of-experts layer. arXiv preprint arXiv:1701.06538 (2017)
- [21] Behringer, D.W., Ji, M., Leetmaa, A.: An improved coupled model for enso prediction and implications for ocean initialization. part i: The ocean data assimilation system. *Monthly Weather Review* **126**(4), 1013–1021 (1998)
- [22] Luo, J.-J., Masson, S., Behera, S., Shingu, S., Yamagata, T.: Seasonal climate predictability in a coupled oagcm using a different approach for ensemble forecasts. *Journal of climate* **18**(21), 4474–4497 (2005)
- [23] Huihang, S., Yiguo, W., Jingjia, L.: Impact of ocean data assimilation on initial conditions and skills of seasonal-to-interannual climate prediction. *Journal of Tropical Oceanography* **41**(3), 75–90
- [24] Kirtman, B.P., Min, D., Infanti, J.M., Kinter, J.L., Paolino, D.A., Zhang, Q., Van Den Dool, H., Saha, S., Mendez, M.P., Becker, E., et al.: The north american multimodel ensemble: phase-1 seasonal-to-interannual prediction; phase-2 toward developing intraseasonal prediction. *Bulletin of the American Meteorological Society* **95**(4), 585–601 (2014)
- [25] Oliver, E.C., Benthuisen, J.A., Darmaraki, S., Donat, M.G., Hobday, A.J., Holbrook, N.J., Schlegel, R.W., Sen Gupta, A.: Marine heatwaves. *Annual review of*

marine science **13**, 313–342 (2021)

- [26] Jacox, M.G., Alexander, M.A., Amaya, D., Becker, E., Bograd, S.J., Brodie, S., Hazen, E.L., Pozo Buil, M., Tommasi, D.: Global seasonal forecasts of marine heatwaves. *Nature* **604**(7906), 486–490 (2022)
- [27] Wernberg, T., Smale, D.A., Tuya, F., Thomsen, M.S., Langlois, T.J., De Bettignies, T., Bennett, S., Rousseaux, C.S.: An extreme climatic event alters marine ecosystem structure in a global biodiversity hotspot. *Nature Climate Change* **3**(1), 78–82 (2013)
- [28] Smith, K.E., Burrows, M.T., Hobday, A.J., Sen Gupta, A., Moore, P.J., Thomsen, M., Wernberg, T., Smale, D.A.: Socioeconomic impacts of marine heatwaves: Global issues and opportunities. *Science* **374**(6566), 3593 (2021)
- [29] McAdam, R., Masina, S., Gualdi, S.: Seasonal forecasting of subsurface marine heatwaves. *Communications Earth & Environment* **4**(1), 225 (2023)
- [30] Ferro, C.A., Stephenson, D.B.: Extremal dependence indices: Improved verification measures for deterministic forecasts of rare binary events. *Weather and Forecasting* **26**(5), 699–713 (2011)
- [31] Trenberth, K.E.: The definition of el nino. *Bulletin of the American Meteorological Society* **78**(12), 2771–2778 (1997)
- [32] Cane, M.A.: The evolution of el niño, past and future. *Earth and Planetary Science Letters* **230**(3-4), 227–240 (2005)
- [33] Gupta, A.S., Jourdain, N.C., Brown, J.N., Monselesan, D.: Climate drift in the cmip5 models. *Journal of Climate* **26**(21), 8597–8615 (2013)
- [34] Irving, D., Hobbs, W., Church, J., Zika, J.: A mass and energy conservation analysis of drift in the cmip6 ensemble. *Journal of Climate* **34**(8), 3157–3170 (2021) <https://doi.org/10.1175/JCLI-D-20-0281.1>
- [35] Richter, I., Tokinaga, H.: An overview of the performance of cmip6 models in the tropical atlantic: mean state, variability, and remote impacts. *Climate Dynamics* **55**(9), 2579–2601 (2020)
- [36] Zhang, Q., Liu, B., Li, S., Zhou, T.: Understanding models’ global sea surface temperature bias in mean state: from cmip5 to cmip6. *Geophysical Research Letters* **50**(4), 2022–100888 (2023)
- [37] Eyring, V., Bony, S., Meehl, G.A., Senior, C.A., Stevens, B., Stouffer, R.J., Taylor, K.E.: Overview of the coupled model intercomparison project phase 6 (cmip6) experimental design and organization. *Geoscientific Model Development* **9**(5), 1937–1958 (2016)



- [38] Carton, J.A., Chepurin, G., Cao, X., Giese, B.: A simple ocean data assimilation analysis of the global upper ocean 1950–95. part i: Methodology. *Journal of Physical Oceanography* **30**(2), 294–309 (2000)
- [39] Copernicus Climate Change Service, C.D.S.: Oras5 global ocean reanalysis monthly data from 1958 to present (2021)
- [40] Hobday, A.J., Alexander, L.V., Perkins, S.E., Smale, D.A., Straub, S.C., Oliver, E.C., Benthuisen, J.A., Burrows, M.T., Donat, M.G., Feng, M., *et al.*: A hierarchical approach to defining marine heatwaves. *Progress in oceanography* **141**, 227–238 (2016)
- [41] Jacox, M.G., Alexander, M.A., Bograd, S.J., Scott, J.D.: Thermal displacement by marine heatwaves. *Nature* **584**(7819), 82–86 (2020)
- [42] Dosovitskiy, A., Beyer, L., Kolesnikov, A., Weissenborn, D., Zhai, X., Unterthiner, T., Dehghani, M., Minderer, M., Heigold, G., Gelly, S., *et al.*: An image is worth 16x16 words: Transformers for image recognition at scale. *arXiv preprint arXiv:2010.11929* (2020)
- [43] Liu, Z., Lin, Y., Cao, Y., Hu, H., Wei, Y., Zhang, Z., Lin, S., Guo, B.: Swin transformer: Hierarchical vision transformer using shifted windows. In: *Proceedings of the IEEE/CVF International Conference on Computer Vision*, pp. 10012–10022 (2021)
- [44] Su, J., Ahmed, M., Lu, Y., Pan, S., Bo, W., Liu, Y.: Roformer: Enhanced transformer with rotary position embedding. *Neurocomputing* **568**, 127063 (2024)
- [45] Zhou, L., Zhang, R.-H.: A self-attention-based neural network for three-dimensional multivariate modeling and its skillful ENSO predictions. *Science Advances* **9**(10), 2827 (2023)
- [46] Ba, J.L., Kiros, J.R., Hinton, G.E.: Layer normalization. *arXiv preprint arXiv:1607.06450* (2016)
- [47] Kingma, D.P., Ba, J.: Adam: A method for stochastic optimization. *arXiv preprint arXiv:1412.6980* (2014)

# Supplementary

## Dataset Details

Simulated data from twenty CMIP6 models are selected for training ORCA . The model name and corresponding institution are listed in Table S1. For each model, only one member is selected, i.e., member r1i1p1f3 is used in HadGEM3-GC31-MM, and r1i1p1f1 is used in the others.

Source ID	Institution
BCC-CSM2-MR	Beijing Climate Center
CAS-ESM2-0	Chinese Academy of Sciences
CIESM	Department of Earth System Science, Tsinghua University
CMCC-CM2-HR4	Fondazione Centro Euro-Mediterraneo sui Cambiamenti Climatici
CMCC-CM2-SR5	Fondazione Centro Euro-Mediterraneo sui Cambiamenti Climatici
CMCC-ESM2	Fondazione Centro Euro-Mediterraneo sui Cambiamenti Climatici
E3SM-1-0	E3SM-Project
E3SM-1-1	E3SM-Project
E3SM-2-0	E3SM-Project
EC-Earth3	EC-Earth Consortium
EC-Earth3-Veg	EC-Earth Consortium
FGOALS-f3-L	Chinese Academy of Sciences
FIO-ESM-2-0	First Institute of Oceanography, Ministry of Natural Resources / Qingdao National Laboratory for Marine Science and Technology
HadGEM3-GC31-MM	Met Office Hadley Centre
INM-CM4-8	Institute for Numerical Mathematics, Russian Academy of Science
INM-CM5-0	Institute for Numerical Mathematics, Russian Academy of Science
MPI-ESM1-2-HR	Max Planck Institute for Meteorology / Deutscher Wetterdienst / Deutsches Klimarechenzentrum
MRI-ESM2-0	Meteorological Research Institute
SAM0-UNICON	Seoul National University
TaiESM1	Research Center for Environmental Changes, Academia Sinica

**Table S1** CMIP6 models used for training.

The periods for each dataset used in this work are listed in Table S2. Specifically, the reanalysis data from SODA2 and ORAS5 before 1980 is used for validation in order to avoid data leakage with the testing data.

	Data	Period
Training	CMIP6	1850-2014
Validation	SODA2	1871-1979
	ORAS5	1958-1979
Testing	GODAS	1980-2023

**Table S2** Datasets used in ORCA.

## High-Frequency Regions of Subsurface MHW

The ranges of seven regions used for subsurface MHW forecast are listed in Table S3.

Region	Range
Bering Sea	45°N-60°N, 170°E-170°W
Northeast Pacific	35°N-60°N, 160°W-125°W
Mediterranean Sea	25°N-50°N, 0°E-40°E
Northwest Atlantic	20°N-40°N, 80°W-30°W
South Indian Ocean	40°S-20°S, 60°E-100°W
Tasman Sea	50°S-30°S, 150°E-170°E
Southwest Atlantic	50°S-30°S, 60°W-20°W

**Table S3** The range of each region considered for subsurface MHWs forecast.

## RMSE/ACC Skills in Depths

Fig. S1 and Fig. S2 depict the RMSE and ACC skill for four multi-level ocean variables (thetao, uo, vo, and so), respectively. ORCA performs the best at each depth, which further demonstrates the extraordinary three-dimensional modeling capability.

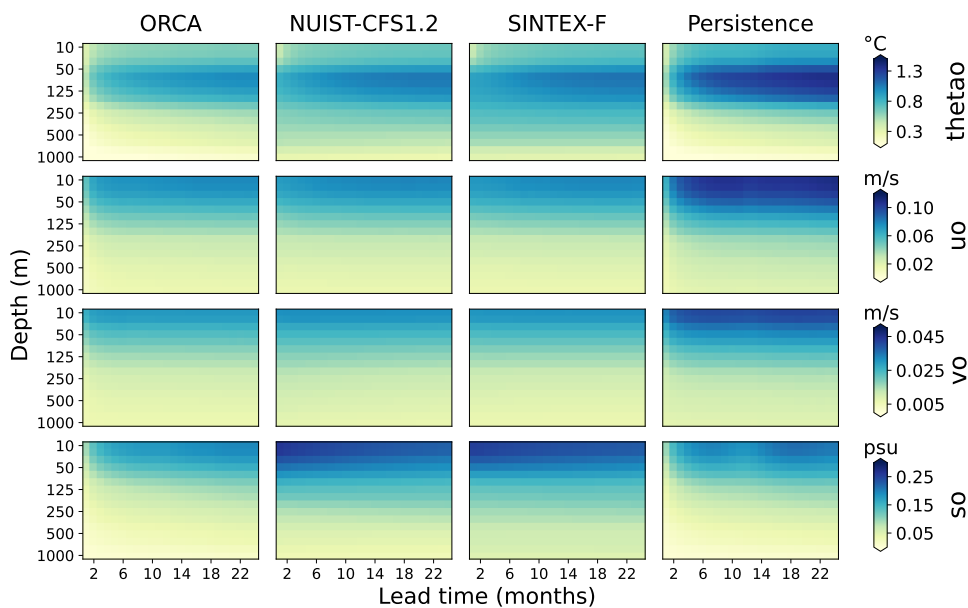


**Fig. S1** The global averaged RMSE of thetato, uo, vo, and so (from top row to bottom row) at each depth (the lower the better). The x-axis and y-axis represent the forecast lead time and depth, respectively. The filled color represents the RMSE. From left to right, each column represents the result from ORCA, NUIST-CFS1.2, and SINTEX-F, respectively.

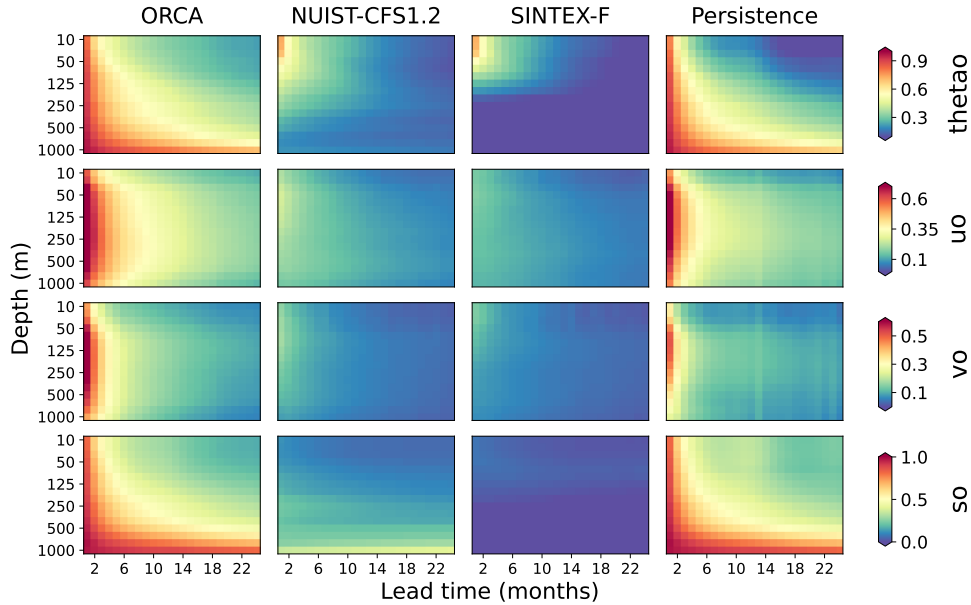


**Fig. S2** The global averaged ACC of  $\theta_{\text{tao}}$ ,  $u_{\text{o}}$ ,  $v_{\text{o}}$ , and  $s_{\text{o}}$  (from top row to bottom row) at each depth (the higher the better). The x-axis and y-axis represent the forecast lead time and depth, respectively. The filled color represents the ACC. From left to right, each column represents the result from ORCA, NUIST-CFS1.2, and SINTEX-F, respectively.

As shown in Fig. S1, the RMSE decreases with the increasing of depth for all models, possibly due to smaller values at deeper levels. The ACC shown in Fig. S2 exhibits a different mode. For  $\theta_{\text{tao}}$  and  $s_{\text{o}}$ , ACC increases with depth, while for velocity, it reaches the best at middle depths and then decreases. The relatively poor performance of shallow velocity prediction may be due to greater uncertainty and lower predictability influenced by the atmosphere. The reason for poor performance at depth may be the poor data quality. Overall, ORCA still outperforms other models at almost all lead time.

### Surface MHWs Forecast

Fig. S3 E shows the frequency distribution of surface MHWs (the definition is similar to the subsurface, except that the surface temperature is used) using the GODAS data. It is not much different from Fig. 2 E, except for the North Central Pacific region. Fig. S3 A-D and F-I illustrate the SEDI skills for global and seven regions with a relatively high frequency of occurrence. ORCA shows the highest performance in almost all cases, especially at long lead time.

### Niño3.4 Index Prediction

Based on the predictions of surface temperature, the Niño3.4 index can be calculated. In Fig. S4 A, we present the prediction skills for Niño3.4 index up to 24

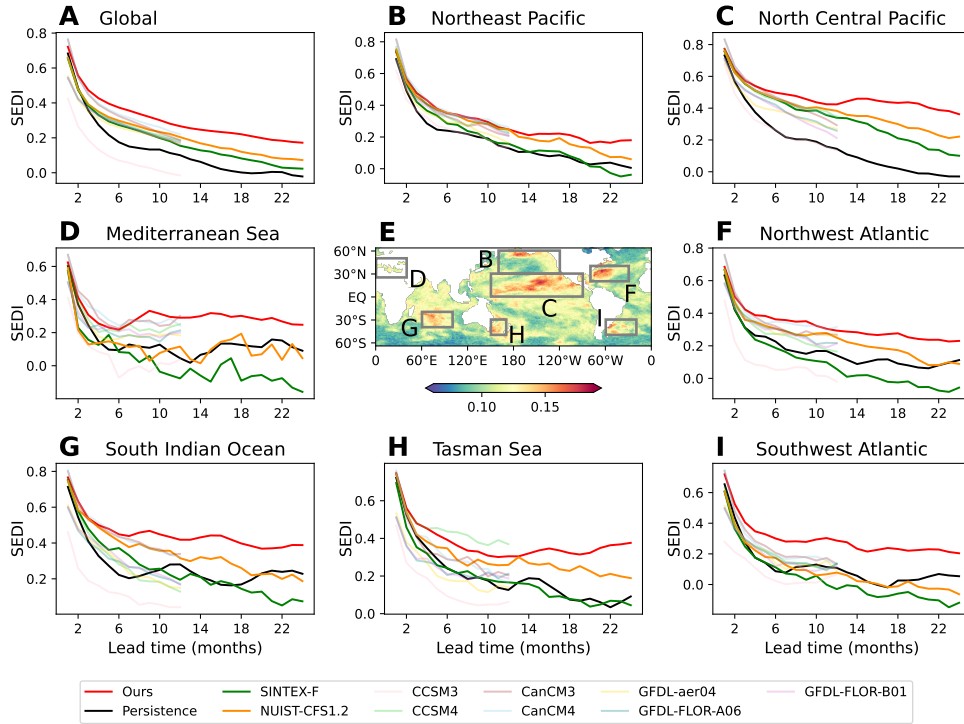


**Fig. S3 Forecast skills of surface marine heatwaves (defined by surface temperature).** (A-D, F-I) The average SEDI for global and seven regions with a relatively high frequency of heat-wave occurrences, the higher the better. The x-axis represents the forecast lead time. (E) Global distribution map of the frequency of heat wave events from GODAS. The area in the gray box corresponds to the surrounding subgraph identified by the black letter. The range of Northeast Pacific and North Central Pacific are (30°N-60°N, 160°E-120°W) and (0°- 30°N, 150°E-90°W), respectively. Other regions keep the same as in Table S3.

months. ORCA outperforms other models by a large margin, especially at the long lead time. Fig. S4 B-D show the ACC skills for prediction of Niño3.4 index targeted to each season. Compared to NUIST-CFS1.2 and SINTEX-F, ORCA exhibits significant advantages across all seasons.

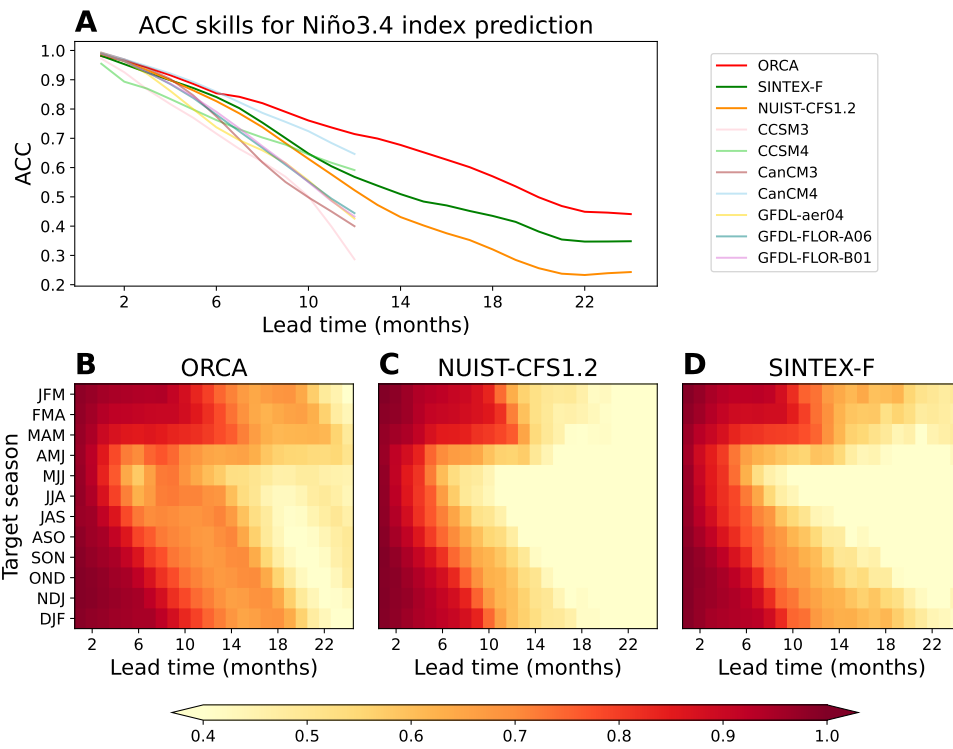


**Fig. S4 Niño3.4 prediction.** (A) The ACC skills for Niño3.4 prediction of ORCA and several dynamical models. (B-D) The ACC skills for prediction of Niño3.4 index targeted to each season in ORCA, NUIST-CFS1.2, and SINTEX-F, respectively.